SAND2022-10242C

Trans-Barrier Communication Device For High Data Rate Applications

1st Celestino A. Corral
Sandia National Laboratories
Livermore, California USA
cacorra@sandia.gov

2nd Charles M. Reinke
Sandia National Laboratories
Albuquerque, New Mexico USA
cmreink@sandia.gov

3rd Christopher L. Gibson
Sandia National Laboratories
Albuquerque, New Mexico USA
cgibson@sandia.gov

4th Ihab F. El-Kady
Sandia National Laboratories
Albuquerque, New Mexico USA
ielkady@sandia.gov

5th Greg B. Haschke
Sandia National Laboratories
Albuquerque, New Mexico USA
gbhasch@sandia.gov

***Abstract*—A high bandwidth piezoelectric transducer technology for high data rate communications across metallic barriers is presented and discussed. To properly characterize the channel, a linear time-invariant (LTI) model of the device is obtained using frequency fitting methods on the S-parameter measurements of the communication network. The corresponding impulse response of the channel is derived from the poles and residues used to fit the frequency data. A recursive formulation of the impulse response of complex poles is advanced and analyzed. The channel characteristics were used to estimate the trans-barrier data rate employing orthogonal frequency division multiplex (OFDM) as used in a powerline communication (PLC) standard. An off-the-shelf PLC system is used to communicate through a metallic barrier and data rates exceeding 70 Mbps were achieved as predicted by the model. The methods described here are useful for estimating the physical data rate achievable by trans-barrier communication systems using piezoelectric transducers.**

***Index Terms*—channel characterization, vector fitting, impulse response, mechanical transduction, powerline communication**

I. Introduction

The idea of providing power and/or communicating across a metal barrier without feedthroughs, holes, or other apertures has gained considerable interest in recent years. The shift from conventional connector technology to trans-barrier energy transfer can provide mechanical isolation between delicate internal electronic components and environmental factors such as thermal stress, pressure, and contaminants. In addition, design for electromagnetic compatibility (EMC) would be greatly simplified as the metal serves as a highly effective shield against conducted and radiated electrical energy.

Sandia National Laboratories is a multimission laboratory managed and operated by National Technology & Engineering Solutions of Sandia, LLC, a wholly owned subsidiary of Honeywell International Inc., for the U.S. Department of Energys National Nuclear Security Administration under contract DE-NA0003525.

The application space for such technology include down-bore hole sensors for drilling and fracking [1] as well as nuclear waste monitoring [2]. The aeronautics and aerospace field can also benefit from trans-barrier energy transfer [3]. As a result, several approaches have been considered for transferring power and data through metallic barriers [4] [5]. In particular, piezoelectric transducers in combination with orthogonal frequency division multiplex (OFDM) communication scheme have achieved data rate performance of 12 [6] [7], 15 [8] [9] and $>$ 17 Mbps [10].

OFDM is a discrete multi-tone technique where a large number of orthogonally spaced narrowband carriers are independently modulated and processed. Highly variable frequency response can be accommodated by OFDM through a variety of techniques. Due to the spectral efficiency of OFDM, higher data rates can be achieved by developing transducers with larger bandwidth. Sandia National Laboratories has developed novel piezoelectric transducers based on lead zirconate titanate (PZT) that have a sufficiently high mechanical frequency while also being fairly agnostic to barrier material and thickness. However, the complex physical phenomena of the piezoelectric transducer operation is difficult to model, so estimating communication performance is challenging.

In this paper a systematic approach for characterizing and modeling a trans-barrier communication channel based on its S-parameter frequency measurements is proposed. The method consists of approximating the frequency response using two different frequency fit methods for comparison purposes. The causal channel impulse response (CIR) of the channel is then determined from the complex poles and residues of the fitted transfer function. A recursive formula for the portion of the impulse response due to complex poles is advanced and analyzed. An estimate of the channel delay through the barrier is used to set the parameters using the HomePlug powerline communication (PLC) OFDM-based standard [11]. An off-the-shelf PLC system with similar capability is used for the communication tests. It is shown that data rates exceeding 70 Mbps can be achieved in trans-barrier communications.

II. Device Characterization

The transducers exploit the piezoelectric effect which is the accumulation of electrical charge in the material in response to applied mechanical stress [12]. The piezoelectric material is not conductive on its own. However, when the device is exposed to mechanical stress, a shifting of the positive and negative charge centers in the material takes place, resulting in an external field that encodes the information. Therefore, the main electrical transfer of energy is through voltage modulation, and we are interested in characterizing the trans-barrier communication system using the voltage transfer function.

The communication test system utilizes a pair of piezoelectric transducers co-axially aligned and directly coupled to opposite sides of a wall common to the aluminum enclosures as shown in Figure 1. The enclosures provide effective electromagnetic isolation over the frequency range of the tests. Shielded RF cables feed the signal to the respective devices inside the enclosures for frequency response characterization.

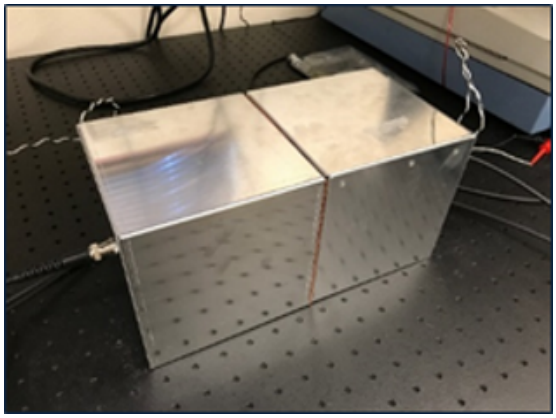

Fig. 1. Device frequency measurement setup showing aluminum Faraday cages butted together and corresponding signal ports. Each transducer is inside the respective cage connected to the barrier that is common to the enclosures.

We assume the transducer is electrically well-defined by a linear time-invariant (LTI) filter channel model where the output response $r(t)$ of the channel in time is characterized by the following relation [13]

$$r(t) = s(t) \otimes h(t) + n(t) = \int_{-\infty}^{+\infty} s(\tau) h(t-\tau) d\tau + n(t) \quad (1)$$

In (1) $s(t)$ is the signal, $h(t)$ is the impulse response of the LTI channel, $n(t)$ is the noise, and $\otimes$ denotes the convolution operator. The channel impulse response $h(t)$ is the time-domain representation of the channel's frequency transfer function $H(j\omega)$ relating the output voltage to the input voltage as a function of frequency $\omega = 2\pi f$.

A vector network analyzer (VNA) measured the two-port S-parameters of the channel. S-parameter measurements describe device characteristics in terms of incident and reflected electrical waves. The voltage transfer function is related to the two-port S-parameters via the relation [14]

$$A_V = \frac{S_{21}(1+\Gamma_L)}{(1-S_{22}\Gamma_L) + S_{11}(1-S_{22}\Gamma_L) + S_{12}S_{21}\Gamma_L} \quad (2)$$

where Γ_L is the load reflection coefficient. Network analyzer S-parameter measurements are performed in properly terminated loads so $\Gamma_L = 0$ and (2) becomes $A_V = S_{21}/(1+S_{11})$. This is the resulting transfer function $H(j\omega)$.

There are several electrical properties we can determine from the S-parameters in relation to device characteristics. One property is *Reciprocity* given by the relation

$$S = S^T \quad \text{or} \quad S_{ji} = S_{ij} \quad \text{for } i \neq j \quad (3)$$

If a network is reciprocal it can imply that linear reciprocal materials are used in the device. Another property is *Symmetry* given by

$$S_{ii} = S_{jj}, \quad \text{for } i \neq j \quad (4)$$

Symmetrical networks are often physically symmetrical, but this need not be the case in general. Both of these properties are checked as part of characterizing the device.

Another important property is *Passivity*. Passivity has been shown to be the most stringent requirement of an electrical network as it implies both causality and stability [15]. Passivity can be confirmed directly from the S-parameters by checking the condition

$$\text{eig}[I - S^*S] \geq 0 \Rightarrow \text{eig}[S^*S] \leq 1 \quad (5)$$

where eig$[M]$ refers to the eigenvalues of the matrix M. Any frequencies that violate this condition must be further analyzed in relation to the measured data to understand the nature of the violation.

One final consideration is that the time-domain response of the device must be causal. For causality, $S_{ij}(t) = 0$ for $t < T_{ij}$ with $T_{ij} > 0$; that is, the network cannot have a response before any stimulus is applied. There are means of validating the causality of the system theoretically. The Kramers-Kronig relations [16] are directly applicable to the real and imaginary parts of the measured S-parameters. On the other hand, the Paley-Wiener [17] can be used with the frequency-domain transfer function from (2). As noted earlier, passivity implies causality, so the passivity tests are sufficient for our case.

For proper communication system design, the channel impulse response (CIR) is needed from the frequency-domain measured data. However, there are challenges with using S-parameter measurements directly in obtaining the channel impulse response. The S-parameters are measured over a finite bandwidth. The truncated frequency response is equivalent to frequency-domain rectangular windowing so the time-domain response is non-causal [18]. To circumvent the causality issue, the work of [19] describes a method for artificially extending the frequency response and maintaining amplitude and phase integrity of the response via the Hilbert transform. We choose to employ vector fitting to approximate the frequency response and extract the causal impulse response as discussed in the next section.

III. Frequency Fitting Methods

The measured S-parameters of the device out to 50 MHz are plotted in Figure 2. The S_{21} frequency response has multiple lobes starting at 5 MHz and spaced roughly 10 MHz apart. The peak of each lobe is approximately 15 dB below the previous lobe peak as the frequency increases. The phase responses are approximately linear with slight bumps coinciding with the nulls of the magnitude response. The input and output return loss are highly reflective throughout most of the band. Over the entire frequency range the device is passive and reciprocal, and nearly symmetric.

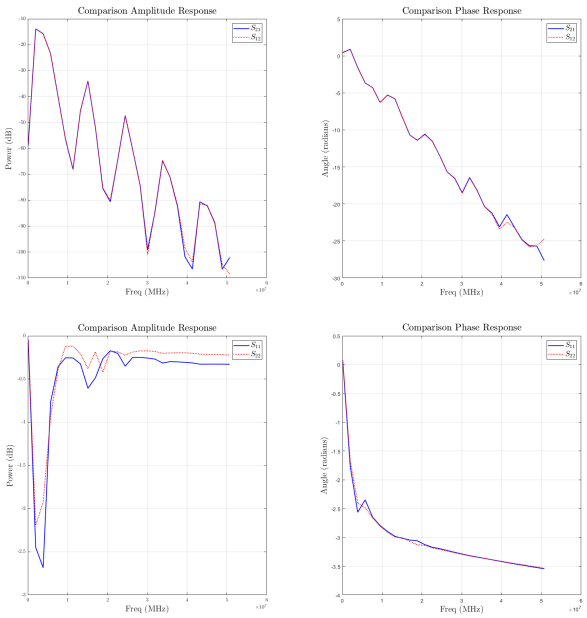

Fig. 2. S-parameter measurements of sample PZT device in frequency range $0 \leq f \leq 50$ MHz over all ports of interest.

We seek to obtain a LTI channel model of the frequency response and extract the channel impulse response from the data. Vector fitting (VF) is a means of fitting a rational function in the complex domain to a complex vector of frequency response data [20] as

$$f(s) = \sum_{k=1}^{N} \frac{c_k}{s - a_k} + d + sh \tag{6}$$

where complex frequency $s = j\omega = j2\pi f$, f is the frequency, c_k and a_k are the residues and poles, respectively, d is some real constant, h is a real value representing a scaling parameter for the fit, and N is the number of poles used to fit the data. The fit is obtained from a sequential solution to (6), estimating the coefficients using a least squares approximation of the function over the selected frequency interval. The vector fitting method has been shown to be robust, accurate, and fairly efficient when compared to other techniques for approximating a frequency response [21]. Matlab supports vector fitting through the `rationalfit` function [22].

Matlab introduced the `rational object` in Matlab R2020a and is described as using an interpolation algorithm to create a rational fit to frequency-dependent data [23]. Like the vector fit (VF) method, this function provides the error to the fit as well as the ability to specify the maximum number of poles N with default being $N = 1000$. The formulation is similar to that of (6) except $h = 0$ and we only retain the direct term d. The direct term is a constant and offers a degree of freedom to improve the fit but may introduce an impulse at $t = 0$.

The `rational object` fit to $A_V = S_{21}/(1 + S_{11})$ magnitude and phase are plotted in Figure 3. The method results in a good fit over the first three lobes. Beyond the third lobe, the amplitude response climbs slightly and then flattens. This is because the number of poles used in this approximation is $N = 16$ which is fairly low but makes the response less sensitive to higher number of poles. The error between the original and fitted magnitude response is -29.9 dB. The phase responses deviate substantially beyond 30 MHz where phase becomes flat. However, the energy contribution beyond this frequency does not play a significant role in the response.

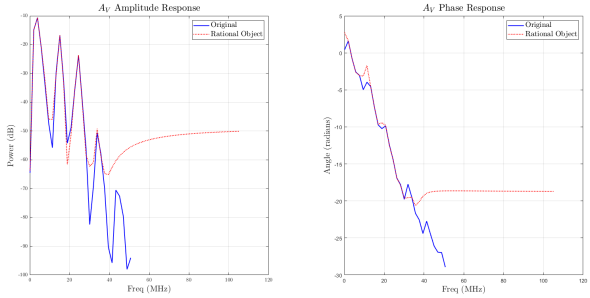

Fig. 3. Plot of rational object fit to voltage transfer function A_V frequency response of the device spectrum in dB and unwrapped phase in radians.

An advantage of using Matlab's `rational object` is that there is the companion function `zpk` that extracts the poles from the object for further analysis [24]. A plot of the pole-zero diagram of the fitted response is given in Figure 4. All poles and zeros are complex conjugate pairs. The poles are all in the left-half plane so the response is stable. There are two zeros near the origin to accommodate the very low amplitude at DC.

The presence of zeros in the right-half plane indicate the fitted function is non-minimum phase. A minimum phase transfer function implies that if the magnitude response of the transfer function is specified so is its phase. A non-minimum phase function violates this relation and has its energy concentrated near the start of the impulse response [25]. In addition, the resulting group delay of the fitted response is not minimum. Therefore, there will be slightly more delay in the impulse response obtained from the `rational object` approximation. We consider this outcome as providing a conservative limit for the channel delay if the device is actually minimum phase.

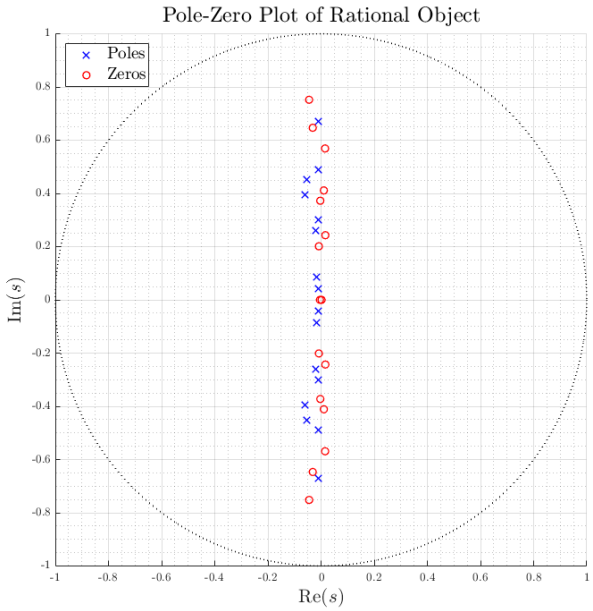

Fig. 4. Pole-zero plot from rational object fit to S-parameter data of device frequency response.

IV. Channel Impulse Response

To obtain the channel impulse response from the vector fit and `rational object` methods, we used Matlab's `timeresp` function [26]. A proper sampling rate was chosen relative to the frequency response of the device. The peak of the impulse response A is obtained by finding the largest value of the response vector. We then chose to find the time t_γ where the impulse response amplitude is γA with $\gamma < 1$. This was done by sorting the impulse response vector and finding the time closest to the desired value γA with $\gamma = 0.1$ for our case. This technique was used to find the relevant parts of the plots shown in this section.

Figure 5 shows the impulse response due to each method. It is evident that the results of the VF and `rational object` methods are very close. The impulse response of the `rational object` method introduces an impulse at $t = 0$ which is not present for the VF method. The peak of the impulse response A occurs at $t_A = 0.17$ μsec and the response decays to 10% of that peak at $t_\gamma = 0.8$ μsec. Note that because the methods are based on the summation of simple poles, it is passive and the response is causal *a fortiori*.

To understand the effects of the impulse response on a signal, it is important to quantify the impulse response duration. The convolution operation given by (1) inverts the impulse response about the time axis and slides across the signal, generating a result that corresponds to the area under of the curve of the overlap between the two. A longer impulse response has more overlap that extends the response at the tail of the signal producing inter-symbol interference (ISI). Higher levels of ISI means communication systems must either

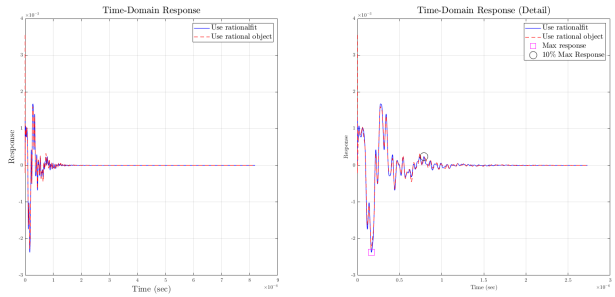

Fig. 5. Plot of channel impulse response from the rational object approach compared to a similar extraction using vector fitting (VF) method. Left plot shows response and right plot shows response detail including maximum of time response and time when response is down 10% from the maximum for VF result.

implement longer symbols or provide more separation between symbols resulting in reduced data rates. To be conservative, we would say that the impulse response has little effect beyond 1.5 μsec.

At this point it is useful to note that the frequency fit methods result in poles that can be real or complex conjugates with the latter captured by the relation

$$\frac{K}{s+\alpha+j\omega}+\frac{K^*}{s+\alpha-j\omega}=2\frac{(s+\alpha)\Re[K]+\omega\Im[K]}{(s+\alpha)^2+\omega^2}$$

where $\Re[x], \Im[x]$ denote the real and imaginary parts of x, respectively, the complex frequency is denoted by $\alpha + j\omega$, K is the residue, and K^* is the complex conjugate of K. It is well known that rearranging the formulation and evaluating the inverse Laplace transform yields the total impulse response as [27]

$$h(t)=2\sum_{i=1}^{k}|K_{2i-1}|e^{-\alpha_{2i-1}t}\cos(\omega_{2i-1}t-\arg[K_{2i-1}])U_{-1}(t) + \sum_{i=k+1}^{N}K_i e^{-p_i t}U_{-1}(t) \tag{7}$$

where

$$U_{-1}(t)=\begin{cases}0, & t<0\\ 1, & t>0\end{cases}$$

is the unit step function. We can see that the response consists of contributions from real poles and conjugate complex poles and is a well-known result of passive network theory. It is noteworthy that (7) is implemented in Matlab's `impulse` function for a `rational fit` object.

Now let us turn our attention to the channel response captured in (7), in particular, the portion corresponding to exponentially decaying sinusoids. It can be shown that the sum of sinusoids is also a sinusoid; that is,

$$\sum_{i=1}^{N}A_i\sin(\omega_i t+\phi_i)=A_C\sin(\omega_C t+\phi_C) \tag{8}$$

when generated recursively. Letting $k \geq 3$ and given the first two sinusoids, the recursion is given by the following relations

$$A_k^2 = A_{k-2}^2 + A_{k-1}^2 + 2A_{k-2}A_{k-1}\cos[(\omega_{k-2} - \omega_{k-1})t + (\phi_{k-2} - \phi_{k-1})] \tag{9}$$

$$\omega_k = \frac{\omega_{k-2} + \omega_{k-1}}{2} \tag{10}$$

$$\phi_k = \frac{\phi_{k-2} + \phi_{k-1}}{2} + \Phi \tag{11}$$

$$\Phi = \tan^{-1}\left(\frac{(A_{k-2} - A_{k-1})\sin(\rho)}{(A_{k-2} + A_{k-1})\cos(\rho)}\right) \tag{12}$$

$$\rho = \left(\frac{\omega_{k-2} - \omega_{k-1}}{2}\right)t + \frac{\phi_{k-2} - \phi_{k-1}}{2} \tag{13}$$

Note that the amplitudes are exponentially decaying; that is, for any A_i we actually have $A_i \exp(-\beta_i t)$. This recursion shows that the impulse response of a LTI system based on complex poles can be represented by a single sinusoid with time-varying amplitude and phase.

There are some interesting implications of this result. First, the amplitude A_C is the envelope of the resulting sinusoid. It is the sum of slowly varying sinusoids with time-varying phase. Given an arbitrary set of values for A_i, ω_i, ϕ_i, the resulting envelope is the same regardless of the order of the variables in the recursion.

The frequency ω_k in the recursion is not a function of time and is determined from a type of averaging of the frequencies. However, the final frequency ω_C in the sinusoid depends on the order of the values of the recursion and can be different. Thus, if there are m different frequencies, there are $m!$ different final frequencies possible for an equivalent representation. On the other hand, the final phase ϕ_C is a function of time and is also determined from an averaging process. As we shall now discuss, there is an implicit relation between the frequency ω_C and phase ϕ_C for any operation taken to obtain the final frequency and phase relations.

Let us assume that we have obtained a pair (ω_A, ϕ_A) and (ω_B, ϕ_B) with $\omega_A \neq \omega_B$ and $\phi_A \neq \phi_B$ resulting from employing the recursion using a different order of arbitrary values of A_i, ω_i, ϕ_i. Since the amplitudes are the same we can make $A = 1$ without loss of generality, then the following must hold

$$\sin(\omega_A t + \phi_A) = \sin(\omega_B t + \phi_B) \tag{14}$$

From the trigonometric identities we have

$$\sin(X) - \sin(Y) = 2\cos\left(\frac{1}{2}(X+Y)\right)\sin\left(\frac{1}{2}(X-Y)\right) \tag{15}$$

The rightmost term must be zero so that

$$\sin\left(\frac{1}{2}(X-Y)\right) = 0 \Rightarrow \frac{1}{2}(X-Y) = \sin^{-1}(0) = \pm k\pi \tag{16}$$

for $k = 0, 1, \ldots$. Making the appropriate substitution we obtain the condition that the phases must satisfy

$$\phi_A - \phi_B = \pm 2k\pi - (\omega_B - \omega_A)t, \quad k = 0, 1, \ldots \tag{17}$$

The recursion forces this condition for any order of the summation of the sinusoids.

V. Device Communication Performance

The usable bandwidth of the piezoelectric transducers through the metal barrier is generally below 50 MHz, so powerline communication (PLC) technology up to 30 MHz is suitable for this application. To estimate potential data rate performance, the HomePlug PLC standard was used [11]. This standard employs OFDM with 1155 subcarriers between 2 and 30 MHz; the subcarrier spacing is 24.414 kHz corresponding to a symbol length of 40.96 μsec. The cyclic prefix for the OFDM symbol was set to 7.56 musec to comfortably handle the 1.5 μsec delay of the channel; the total symbol length is 48.52 μsec.

The HomePlug standard uses binary phase shift keying (BPSK) and quadrature amplitude modulation (QAM), supporting bit loading up to 12 bits per carrier (corresponding to QAM-4096). Turbo convolutional coding is used at $8/9$ rate and the potential data rate exceeds 200 Mbps. A computational model was developed to perform the bit loading based on the mapping of the subcarrier to the voltage transfer function of Figure 2. The noise floor was assumed to be 60 dB below the peak of the frequency response. Using these parameters, the estimated data rate was 68 Mbps.

To perform the actual trans-barrier communication testing, Sandia acquired a BlueChip Dolphin evaluation kit [28] that uses a combination of IEEE 1901 and ITU-G.9905 standards with an OFDM physical layer. The Bluechip system uses pulse amplitude modulation (PAM) and low density parity check (LDPC) coding with bit loading depending on channel conditions. The frequency response is from 2 to 28 MHz and up to 200 Mbps data rate is possible.

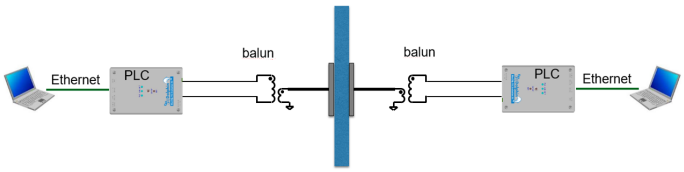

Fig. 6. Drawing showing laptops connected to BlueChip PLC units for throughput tests through a metallic barrier.

Two laptops were set up and the eval kit units were used to drive the piezoelectric transducers through baluns for signal transmission as shown in Figure 6. The Bluechip toolset was used to evaluate the data rate performance through the barrier. Modulation ranged from differential 2-PAM to 16-PAM; 32-PAM was disabled. LDPC code rate $4/5$ was implemented. BlueChip's internal tool for plotting the carrier to interference plus noise ratio (CINR) was used to show the spectrum with bit loading in Figure 7. The raw data rate was about 76 Mbps with lossless packet data rate of 43 Mbps. This is in good agreement with the estimation based on the HomePlug parameters.

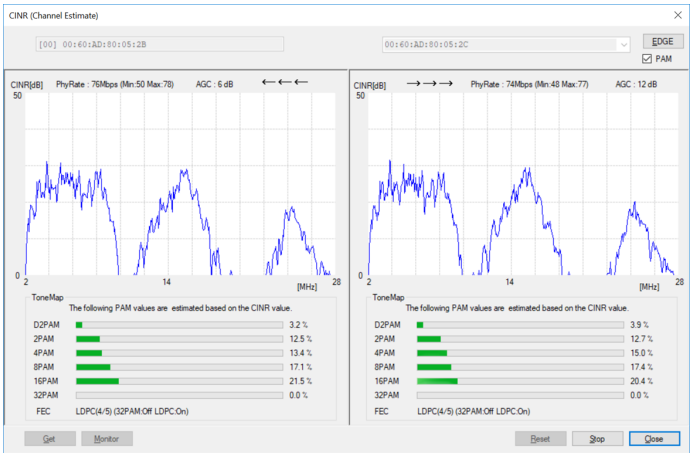

Fig. 7. Capture from BlueChip's tool showing CINR over 2 to 28 MHz spectrum with corresponding bit loading and data rates.

VI. Summary and Considerations

We have presented a systematic approach to characterizing and designing for a high data rate communication system across metallic barriers using piezoelectric transducers. By using frequency fitting on the measured S-parameters of the channel we extract a causal channel impulse response and use the time-domain characteristics to set the appropriate parameters for the communication system. For our application we used OFDM and the HomePlug powerline communication standard to obtain an estimate of the trans-barrier communication data rate. The use of an off-the-shelf PLC system confirmed raw data rate exceeding 70 Mbps was achievable, very close to the estimate.

It is possible to deploy more than one piezoelectric transducer with multi-input multi-output (MIMO) OFDM to achieve more flexible communications options. Transmit diversity can result in superior signal-to-noise ratio across the metallic barrier with corresponding higher data rates. In this case, the connector *enhances* the signal characteristics through the channel. On the other hand, spatial multiplexing can be used to create dedicated communication channels to separate assets within a metallic enclosure. Here, each tile becomes an independent connector, and proper tiling can minimize crosstalk between the transducers.

If a single tile is used for lower data rate communication, the high bandwidth capability of Sandia's piezoelectric transducers can be very useful. For example, it may be possible to emulate a multi-pin device by exploiting orthogonal frequency division multiple access (OFDMA) instead of OFDM. OFDMA allows for the assignment of groups of subcarriers to individual assets requiring lower data rates. The result is a type of "universal" connector with "virtual pins" that isolate devices through the frequency selectivity afforded by the grouped subcarriers. Thus, communication between different assets is possible through a metallic barrier using this approach in lieu of multiple transducers in a tiled configuration.

References

[1] P. Tubel, C. Bergeron and S. Bell, "Mud pulser telemetry system for down hole measurement-while-drilling," *Conference Record IEEE Instrumentation and Measurement Technology Conference*, pp. 219-223, 1992.

[2] A. Pappalardo et al., "An online monitoring system for nuclear waste storage," *2009 1st International Conference on Advancements in Nuclear Instrumentation, Measurement Methods and their Applications*, pp. 1-4, 2009.

[3] M. Kluge, T. Becker, J. Schaik, and T. Otterpohl, "Remote acoustic powering and data transmission for sensors inside of conductive envelopes," *IEEE Sensors 2008*, pp. 41–44, Dec. 2008.

[4] D. J. Graham, J. Neasham, and B. S. Sharif, "Investigation of methods for data communications and power delivery through metals," *IEEE Trans. Ind. Electron.* vol. 58, pp. 4972–4980, 2011.

[5] D-X. Yang, Z. Hu, H. Zhao, H-F. Hu, Y-Z. Sun, and B-J. Hou, "Through-Metal-Wall power delivery and data transmission for enclosed sensors: A Review," *Sensors (Basel, Switzerland)*, vol. 15, pp. 31591–31605, Dec. 2015.

[6] M. Bielinski, K. Wanuga, R. Primerano, M. Kam, and R. Dandekar, "Application of adaptive OFDM bit loading for high data rate through-metal communication," *IEEE Global Telecommunications Conf. (GLOBECOM)* pp. 1–5, 2011.

[7] T. J. Lawry, et al., "Penetration-free system for transmission of data and power through solid metal barriers," *Military Commun. Conf. (MILCOM)*, pp. 389–395, 2011.

[8] K. Wanuga, M. Bielinski, R. Primerano, M. Kam, and K. R. Dandekar, "High-data-rate ultrasonic through-metal communication," *IEEE Trans. Ultrason. Ferroelectr. Freq. Control*, vol. 59, pp. 773–781, July 2003.

[9] Y. Hu, X. Zhang, J. Yang, and Q. Jiang, "Transmitting electric energy through a metal wall by acoustic waves using piezoelectric transducers," *IEEE Trans. Ultrason. Ferroelectr. Freq. Control*, vol. 50, pp. 773–781, July 2003.

[10] T. J. Lawry, K. R. Wilt, J. D. Ashdown, H. A. Scarton, and G. J. Saulnier, "A high-performance ultrasonic system for the simultaneous transmission of data and power through solid metal barriers," *IEEE Trans. Ultrasonics, Ferroelectrics, and Freq. Control*, vol. 60, pp. 194–203, Jan. 2013.

[11] https://en.wikipedia.org/wiki/HomePlug

[12] https://www.nanomotion.com/piezo-ceramic-motor-technology/piezoelectric-effect/

[13] J. G. Proakis, *Digital Communications*, 4th Ed., Boston: McGraw-Hill, 2001, Chapter 1.

[14] G. Gonzalez, *Microwave Transistor Amplifiers—Analysis and Design*, 2nd Ed., Upper Saddle River: Prentice-Hall, 1997.

[15] P. Triverio, *et al.*, "Stability, causality, and passivity in electrical interconnect models," *IEEE Trans. Advanced Packaging*, vol. 30, pp. 795–808, Nov. 2007.

[16] J. Bechhoefer, "Kramers-Kronig, Bode, and the meaning of zero," *Ameri. J. Physics*, vol. 79, pp. 1053–1059, October 2011.

[17] R. E. A. C. Paley and N. Wiener, "Fourier transform in the complex domain," *Ameri. Math. Soc. Collq. Publ.*, vol. 19, Chapter 1, pp. 16–17, 1934.

[18] https://www.simberian.com/Presentations/Shlepnev_S_ParameterQualityMetrics_July2014_final.pdf

[19] F. Rao, "Optimization of spectrum extrapolation for causal impulse response calculation using Hilber transform," *U.S. Pat. 7962541*, June 2011.

[20] B. Gustavsen and A. Semlyen, "Rational approximation of frequency domain responses by vector fitting," *IEEE Trans. Power Delivery*, vol. 14, pp. 1052–1061, July 1999.

[21] A. C. S. Lima, A. B Fernandes, and S. Carneiro, "Rational approximation of frequency domain responses in the S and Z planes," *IEEE Power Engineering Society General Meeting*, San Francisco, California, vol. 1, pp. 126–131, 2005.

[22] https://www.mathworks.com/help/rf/ug/rationalfit.html

[23] https://www.mathworks.com/help/rf/ug/rational.html

[24] https://www.mathworks.com/help/rf/ug/zpk.html

[25] https://en.wikipedia.org/wiki/Minimum_phase

[26] https://www.mathworks.com/help/rf/ug/timeresp.html

[27] C. S. Lindquist, *Active Network Design with Signal Filtering Applications*, Long Beach, California: Steward & Sons, 1977, Chapter 3.

[28] https://megachips.com/hd-plc/product/